Charge exchange and chemical reactions with trapped Th^{3+}

L. R. Churchill,* M. V. DePalatis, and M. S. Chapman
School of Physics, Georgia Institute of Technology, Atlanta, Georgia 30332-0430, USA
(Received 9 December 2010; published 26 January 2011)

We have measured the reaction rates of trapped, buffer gas cooled Th^{3+} and various gases and have analyzed the reaction products using trapped ion mass spectrometry techniques. Ion trap lifetimes are usually limited by reactions with background molecules, and the high electron affinity of multiply charged ions such as Th^{3+} make them more prone to loss. Our results show that reactions of Th^{3+} with carbon dioxide, methane, and oxygen all occur near the classical Langevin rate, while reaction rates with argon, hydrogen, and nitrogen are orders of magnitude lower. Reactions of Th^{3+} with oxygen and methane proceed primarily via charge exchange, while simultaneous charge exchange and chemical reaction occurs between Th^{3+} and carbon dioxide. Loss rates of Th^{3+} in helium are consistent with reaction with impurities in the gas. Reaction rates of Th^{3+} with nitrogen and argon depend on the internal electronic configuration of the Th^{3+}.

DOI: 10.1103/PhysRevA.83.012710 PACS number(s): 34.70.+e, 82.30.Fi

I. INTRODUCTION

Unlike most atomic nuclei, which have excitation energies in the range of kiloelectron volts to megaelectron volts, the nucleus of the thorium isotope, ^{229}Th, has an excited state just several eV above the nuclear ground state [1]. The transition between the nuclear ground state and this unique isomeric state lies within the UV optical spectrum, where it can be addressed using coherent light sources. The coherent control of the electronic states of atoms with tunable lasers has been a major focal point of modern atomic physics. Extending this paradigm to the control of nuclear states of atoms would represent a significant achievement. The transition between the ^{229}Th nuclear states could potentially be used as a frequency reference with a fractional uncertainty approaching 10^{-20} [2]. Furthermore, the transition may be especially sensitive to changes in the value of the fine structure constant, allowing up to 5–6 orders of magnitude enhancement in measurements of its time variation [3]. However, this latter point requires further study [4–7].

In order to demonstrate coherent control of the nuclear state, thorium atoms must be confined in such a way that they can be continuously interrogated and observed. Unlike the lower ionization states, triply ionized thorium has a convenient level structure for fluorescence detection and laser cooling [2]. The low-lying electronic states of Th^{3+} and the optical transitions between them are shown in Fig. 1. Using the more common thorium isotope, ^{232}Th, our group has demonstrated the creation, trapping, and laser cooling of Th^{3+} [8].

In our earliest observations of $^{232}Th^{3+}$, the ions would remain in the trap for only a few seconds. In general, elastic collisions with background molecules are not likely to result in ejection of ions due to the large depth of an ion trap. The primary modes of Th^{3+} loss are charge exchange and chemical reactions with background gases. By improving the background vacuum and increasing the purity of the buffer gas used for initial cooling, we were able to extend the trap lifetime of Th^{3+} to minutes. By removing the buffer gas immediately after the initial trap loading and laser cooling the ions, a lifetime of >10 min was obtained [8].

The limited Th^{3+} trap lifetime presents a significant challenge in time-intensive experiments like measuring the hyperfine states of $^{229}Th^{3+}$ and searching for the nuclear isomer transition. Furthermore, the short lifetime represents a tremendous cost in performing experiments with $^{229}Th^{3+}$ given the extraordinary price of the isotope (>100 k/mg).

To better understand the charge exchange and chemical reaction processes and quantify their rates, we conducted a series of experiments to determine the reaction rate coefficients between Th^{3+} and various gases. A summary of the experimental results can be found in Table I. The remainder of this article is devoted to describing these experiments in greater detail.

A schematic of the ion trap used in these experiments is shown in Fig. 1. The trap is outfitted with a channel electron multiplier (CEM) for electronic detection of trapped ions. When used in combination with the well understood mass selection characteristics of a linear ion trap, the CEM can be used to determine if a specific species of ion is present in the trap.

The ion trap is loaded with Th^{3+} via laser ablation of a thorium metal target with the third harmonic of a pulsed Nd:YAG laser ($\lambda = 355$ nm). The target is located near the trap axis and oriented perpendicular to it. The voltage on the dc endcap nearest the ablation target is gated with the ablation pulse, dropping to ground when the pulse is fired, and increasing to 100 V for ion confinement.

Helium buffer gas is present in the system throughout the loading process. The ablated Th^{3+} ions are initially moving at speeds of 10 km/s as they approach the ion trap. As the hot Th^{3+} ions collide with room temperature helium atoms, they lose some of their thermal energy. This process serves two critical purposes. First, it reduces the energy of some ablated Th^{3+} ions as they traverse the length of the ion trap, thereby increasing the likelihood they will be trapped. Second, it damps the motion of trapped Th^{3+} ions, allowing them to come to thermal equilibrium at some fraction of the trap depth. The helium pressure is commonly held between 10^{-5} and

*Permanent address: Applied Physics Laboratory, Johns Hopkins University, Laurel, MD 20723.

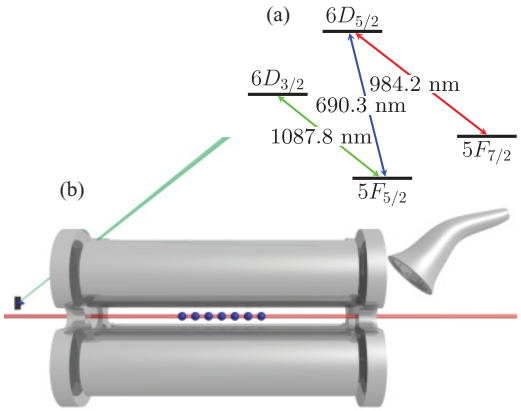

FIG. 1. (Color online) (a) Th^{3+} energy levels and optical transitions. (b) Schematic drawing of ion trap system. A target outside of the ion trap (left) is ablated using the third harmonic of a pulsed Nd:YAG laser (diagonal line). Lasers used for optical excitation of the trapped ions are aligned along the trap axis (horizontal line). A CEM located outside of the trap (right) is used for electronic detection. The CEM is mounted off-axis to allow clear optical access.

10^{-4} torr in these experiments. Generally, the number of ions loaded increases with higher buffer gas pressure, while the final equilibrium temperature of the trapped ions decreases.

II. HELIUM

The loss of Th^{3+} from the ion trap in 5×10^{-5} torr of helium buffer gas is shown in Fig. 2. Here, the Th^{3+} decay rate is measured by observing the reduction in fluorescence over a series of images. This method can be used only when the lifetime of the ions is sufficient to allow enough fluorescence measurements for a proper exponential fit.

When the Th^{3+} trap lifetime is too short for observation of fluorescence, mass selective electronic detection with the CEM is employed to measure the decay rate. We load ions into the trap via ablation and wait for some amount of time. The rf and dc voltages applied to the trap are then tuned such that only Th^{3+} remains stable. The contents of the trap are then delivered to the CEM by lowering the voltage of the trap endcap nearest it. The time interval before the mass selection is varied, and the data are accumulated over several iterations for each time interval. Many iterations are required to suppress the variation due to fluctuations in the number of ions loaded. This method is typically used when the Th^{3+} lifetime is a few seconds or less.

TABLE I. Charge exchange and chemical reaction rate coefficients for Th^{3+}. Reaction rate coefficients are given in units of cubic centimeters per second. Here, k_L is the calculated Langevin rate, and k is the experimental reaction rate coefficient. The corrected reaction rate coefficient is $k_\varepsilon = \varepsilon k$, where ε is the ion gauge correction factor for the gas in question. Experimental reaction rate coefficients for helium and neon are upper bounds. The accuracy of the coefficients given here is limited by the accuracy of the ion gauge used to measure the pressure of the reactants.

Reactant	k	k_ε	(ε)	$k_L \times 10^{-9}$
He	$<3.4 \times 10^{-15}$	$<6.0 \times 10^{-16}$	(0.18)	1.6
Ne	$<4.1 \times 10^{-15}$	$<1.2 \times 10^{-15}$	(0.3)	1.0
Ar*	1.3×10^{-14}	1.7×10^{-14}	(1.3)	1.5
N_2*	1.6×10^{-13}	1.6×10^{-13}	(1.0)	1.8
H_2	4.6×10^{-13}	2.1×10^{-13}	(0.46)	4.4
CH_4	2.6×10^{-9}	3.6×10^{-9}	(1.4)	2.8
O_2	3.7×10^{-9}	3.7×10^{-9}	(1.0)	1.7
CO_2	2.8×10^{-9}	4.0×10^{-9}	(1.4)	1.8

*The reaction rate for Ar and N_2 depends on the electronic configuration of Th^{3+}. The experimental rate refers to reaction from the $5F_{5/2}$ ground state.

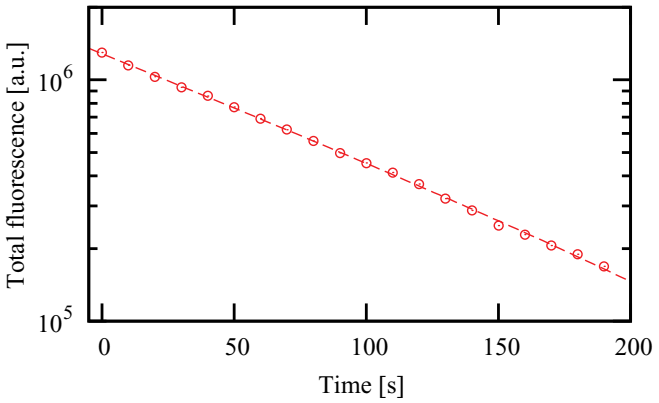

FIG. 2. (Color online) Accumulated fluorescence signal for determination of Th^{3+} loss rate. This data was taken with 5×10^{-5} torr of helium in the vacuum chamber. The loss rate was determined to be $\tau^{-1} = 0.0100(2)\ s^{-1}$.

The decay rate through any given reaction channel is proportional to the density of the reactant in the system. This relation can be written as $\tau^{-1} = kn$, where n is the density of the reactant, and $k = \langle \sigma v \rangle$ is the reaction rate coefficient for the given channel. Here, σ is the reaction cross section and v is the relative velocity between the reactants. For a given reaction, the rate coefficient can be determined by measuring the Th^{3+} decay rate as a function of the pressure of the reactive gas. The reaction rate coefficient is extracted from the slope of a linear fit of this data. The intercept of the linear fit gives the loss rate due to background gases in the vacuum. For helium, the data and corresponding linear fit are shown in Fig. 3.

Helium is a noble gas, and a charge exchange reaction between it and Th^{3+} is endothermic by 4.6 eV. This suggests that such a reaction is strongly inhibited for low-energy reactants. Therefore, the loss shown in Fig. 2 is most likely due to an impurity in the helium rather than to the helium itself.

The helium gas we use in our experiment comes from a cylinder with a built-in purifier (BIP). The BIP helium is supplied by Airgas, Inc. According to the specifications, the BIP helium gas has an impurity level <1 ppm. The data of Fig. 3 implies a reaction rate coefficient between the BIP helium and Th^{3+} on the order of 10^{-16} to 10^{-15} $cm^3\ s^{-1}$. Thus, the reaction between Th^{3+} and the contaminant within the BIP helium responsible for its loss proceeds with a reaction rate coefficient on the order of 10^{-10} to 10^{-9} $cm^3\ s^{-1}$.

A reaction rate coefficient of 10^{-9} $cm^3\ s^{-1}$ is consistent with the value predicted by a classical collision model introduced by Langevin [9] and refined by Gioumousis and Stevenson [10]. This model is helpful in estimating the reaction cross sections

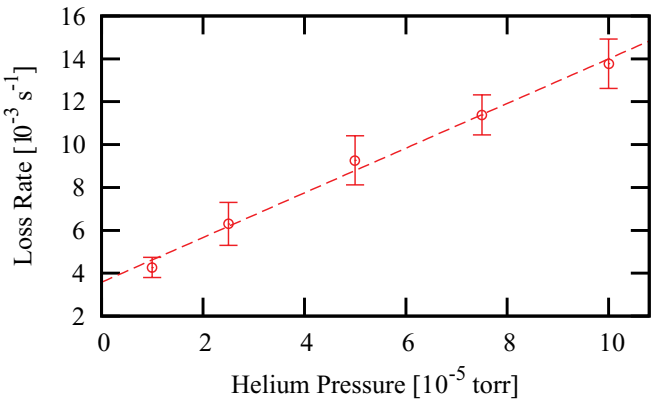

FIG. 3. (Color online) Th^{3+} loss rate as a function of BIP helium buffer gas pressure. The slope of the linear fit implies a reaction rate coefficient of $k = 3.4 \times 10^{-15}$ cm^3 s^{-1} ($k_\epsilon = 6.0 \times 10^{-16}$ cm^3 s^{-1} with an ion gauge correction factor of $\epsilon = 0.18$), while the intercept implies a background loss rate of $\tau^{-1} = 3.3 \times 10^{-3}$ s^{-1}. It is likely that the Th^{3+} reacts with an impurity in the helium rather than with the helium itself; therefore, the value for k sets an upper bound on the reaction rate coefficient for helium.

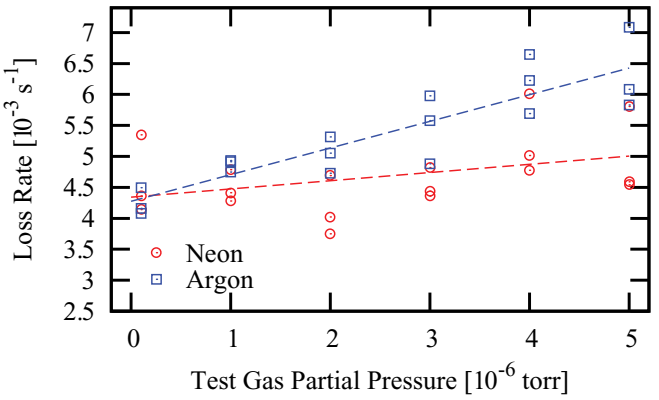

FIG. 4. (Color online) Th^{3+} loss rate in the presence of neon and argon. A partial pressure of 10^{-5} torr of helium was added to the test gas to cool the ions for fluorescence observation. The reaction rate coefficient for neon is $k = 4.1 \times 10^{-15}$ cm^3 s^{-1} ($k_\epsilon = 1.2 \times 10^{-15}$ cm^3 s^{-1} with an ion gauge correction factor of $\epsilon = 0.30$). The decay rates shown for argon represent Th^{3+} loss from the $5F_{5/2}$ ground state. The reaction rate coefficient is $k = 1.3 \times 10^{-14}$ cm^3 s^{-1} ($k_\epsilon = 1.7 \times 10^{-14}$ cm^3 s^{-1} with an ion gauge correction factor of $\epsilon = 1.3$).

between ions and molecules. We assume the ion is a point particle with charge Ze and that the molecule is spherically symmetric with polarizability α. The primary interaction between the ion and molecule is due to the electric field of the ion and the field-induced dipole moment of the molecule. The interaction potential scales as r^{-4}.

Below threshold values of the relative velocity and the impact parameter, the interaction potential leads to a spiraling orbit of the ion and molecule about their shared center of mass. If a reaction between the ion and molecule is exothermic, it is assumed to occur with unit probability when a spiraling orbit occurs. The so-called Langevin cross section for reaction is then [10]

$$\sigma_L = 2\pi \frac{Ze}{v}\sqrt{\frac{\alpha}{\mu}}, \tag{1}$$

where v is the relative velocity between the particles and μ is the reduced mass. The corresponding reaction rate coefficient is

$$k_L = 2\pi Ze\sqrt{\alpha\mu}. \tag{2}$$

The preceding equations are given in Gaussian (cgs) units, which is how they are most commonly found in the literature.

The Langevin model is not a comprehensive theoretical formulation, and therefore, it suffices only to provide an estimate of the reaction rate between a given ion and reactant molecule. The model does not apply to molecules that possess a permanent dipole moment. In that case, the leading term in the interaction potential scales as r^{-2} rather than r^{-4} [11]. Furthermore, several experiments [12–14] have shown a departure from the inverse velocity dependence of the classical cross section in some reactions. Ultimately, the probability of a reaction occurring in the event of a classical interaction is dependent on the combined energy state of the reactants, the available energy states in the final products, and the possible reaction pathways between them [15]. Several experiments [16–20], including our own, have found that some reaction rates can differ significantly depending on the internal energy state of a reactant.

Nevertheless, the Langevin rate is useful in setting an upper bound on the reaction rate between ions and nonpolar molecules [21]. Many ion-molecule reactions do occur at or near the Langevin rate [17,22–26]. The Langevin rates for the reactions we investigated are given in Table I with the experimental results.

III. GASES WITH LOW REACTION RATES

Loss rates of Th^{3+} in the presence of neon and argon are shown in Fig. 4, while loss rates in the presence of nitrogen and hydrogen are shown in Fig. 5. For all of these decay measurements, a partial pressure of 10^{-5} torr of helium was added to the system to cool the ions for fluorescence imaging. As can be seen from Fig. 3, this quantity of helium does not add significantly to the background loss rate of Th^{3+}. The reactions with argon, nitrogen, and hydrogen all proceed relatively slowly, with reaction rate coefficient orders of magnitude below the corresponding Langevin rates. Since our interest was in gases that react with Th^{3+} near the Langevin rate, we did not attempt to identify the products of these reactions.

Like helium, neon is a noble gas with a high ionization energy that inhibits charge exchange reactions with Th^{3+}. Such reactions are in this case endothermic by 1.6 eV. As can be seen in Fig. 4, Th^{3+} loss rates in neon were never significantly larger than what could be attributed to the presence of the helium buffer gas. In addition, the reaction rate coefficient we determined from the data is consistent with reaction occurring between the Th^{3+} and 0.5 ppm impurity in the gas.

It is worth noting that the kinetic energy of Th^{3+} due to rf micromotion could conceivably contribute to overcome an otherwise endothermic energy gap [27–29], such as with helium and neon. However, such micromotion-enhanced reactions would require micromotion amplitudes much larger than is likely. While some contribution of the micromotion to the

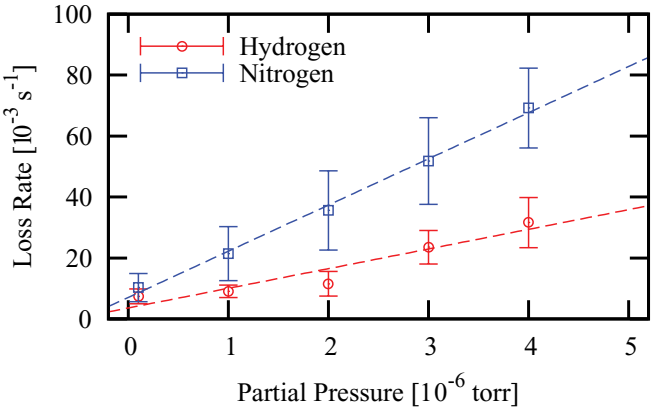

FIG. 5. (Color online) Th^{3+} loss rate in the presence of hydrogen and nitrogen. A partial pressure of 10^{-5} torr of helium was added to the test gas to cool the ions for fluorescence observation. The reaction rate coefficient for hydrogen is $k = 4.6 \times 10^{-13}$ cm^3 s^{-1} ($k_\epsilon = 2.1 \times 10^{-13}$ cm^3 s^{-1} with an ion gauge correction factor of $\epsilon = 0.46$). The decay rates shown for nitrogen represent Th^{3+} loss from the $5F_{5/2}$ ground state. The reaction rate coefficient is $k = 1.6 \times 10^{-13}$ cm^3 s^{-1}.

loss rates is possible for endothermic reactions, our results are consistent with quoted impurities [30].

Argon is also a noble gas, but a charge exchange reaction between it and Th^{3+} is exothermic by 4.2 eV. The Th^{3+} reaction rates with argon and nitrogen were found to depend on the electronic configuration of the Th^{3+}. The data in Fig. 4 represent loss rates from the $5F_{5/2}$ ground state of Th^{3+}. The $5F_{5/2}$ state was isolated for study by shuttering the 690-nm laser between fluorescence measurements. This allows Th^{3+} in the Λ manifold (see Fig. 1) to be pumped back into the ground state by the 984-nm laser. By keeping the time between measurement sufficiently long, the systematic effect introduced during measurement was held below 10%.

IV. Th^{3+} EXCITATION EFFECTS ON REACTION RATES

State-dependent effects on electron capture in collisions between neutral atoms and multiply charged ions have been studied extensively (see, e.g., Refs. [31–34]). The effect of Th^{3+} optical excitation on its reaction rate with argon can be seen clearly in Fig. 6. In one set of measurements, the 690-nm laser was shuttered between fluorescence measurements. This is the same data set shown in Fig. 4. In the other two sets of measurements, the 690-nm laser was left on continuously. Increasing the power of the 984-nm laser increases the population of the $6D_{5/2}$ excited state, and hence the reaction rate, until the excited state is saturated. The corresponding saturation of the argon and nitrogen reaction rates are shown in Fig. 7.

If the $5F_{7/2}$-$6D_{5/2}$ manifold is approximated as a two-level system, the excited state population obeys the relation

$$\sigma \propto \frac{I/I_{\mathrm{sat,eff}}}{1 + I/I_{\mathrm{sat,eff}}}. \tag{3}$$

where $I_{\mathrm{sat,eff}}$ is the effective saturation intensity. The ratio of the effective saturation intensity to the natural saturation intensity, $I_{\mathrm{sat}} = 2\pi^2 hc\Gamma/3\lambda^3$, is approximately equal to the ratio of the

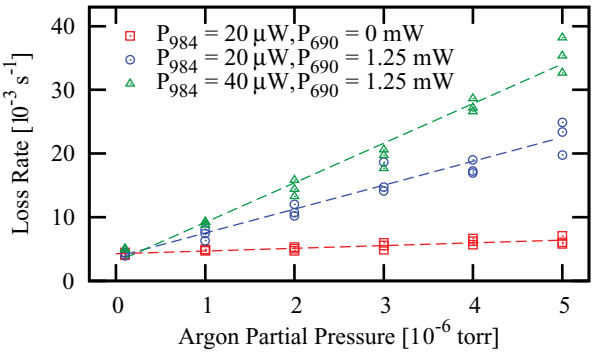

FIG. 6. (Color online) Effect of atomic excitation on Th^{3+} loss rate in the presence of argon. The data that was taken without 690-nm light represents loss from the Th^{3+} $5F_{5/2}$ ground state. Increasing the power of the 984-nm laser increases the reaction rate by increasing the number of ions in the $6D_{5/2}$ excited state, from which reaction is more likely.

Doppler-broadened linewidth, Γ_D, to the natural linewidth, Γ. Therefore,

$$I_{\mathrm{sat,eff}} \approx \frac{2\pi^2 hc}{3\lambda^3}\Gamma_D. \tag{4}$$

By fitting the data in Fig. 7 to a function in the form of Eq. (3), we find an effective saturation intensity of $I_{\mathrm{sat,eff}} \sim 40$ mW/cm^2. According to Eq. (4), this corresponds to a Doppler-broadened linewidth of $\Gamma_D \sim 300$ MHz, which is

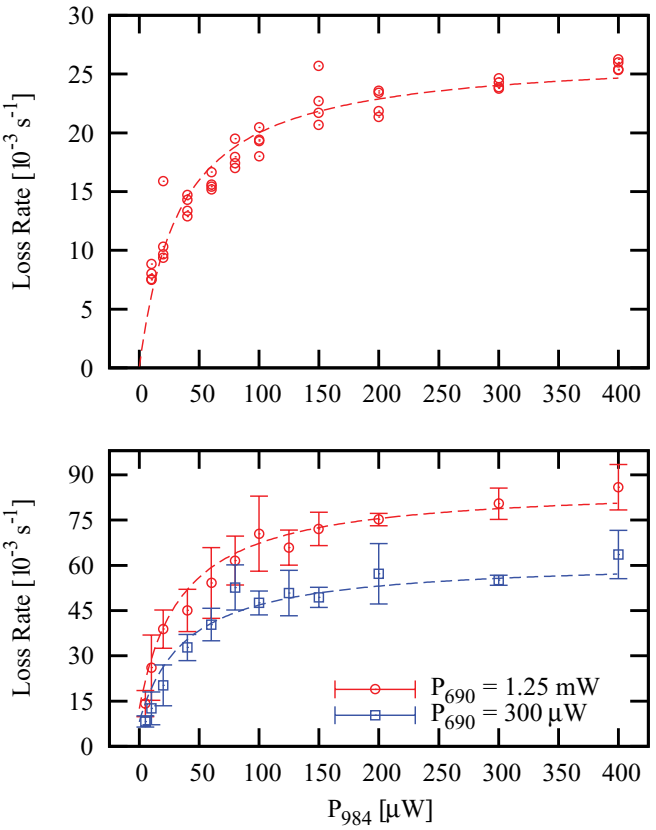

FIG. 7. (Color online) Saturation of Th^{3+} reaction rate in the presence of (top) 3×10^{-6} torr argon and (bottom) 3×10^{-6} torr nitrogen. In each case, 1×10^{-5} torr helium is also present.

consistent with an independent measurement of the transition linewidth.

The reaction rate from the $5F_{7/2}$ electronic state was found to be equal to within experimental error to the reaction rate from the $5F_{5/2}$ state for both argon and nitrogen. The $5F_{7/2}$ state was isolated for measurement by shuttering the 984-nm laser between measurements, while continuously applying the 690-nm laser. In this way, the long-lived $5F_{7/2}$ state was continuously repopulated. To further demonstrate that optical excitation to the $6D_{5/2}$ state was responsible for the increased reaction rates, we verified that detuning the lasers far from resonance had the same effect as shuttering them.

By optically exciting with the 1087-nm laser, we found that reactions with nitrogen were also faster from the $6D_{3/2}$ state than from the $5F_{5/2}$ state. No quantitative comparisons were made between the reaction rates from the $6D_{3/2}$ state and the $6D_{5/2}$ state. The reaction rate between Th^{3+} and argon with 1087-nm optical excitation was not measured.

V. GASES WITH HIGH REACTION RATES

Loss rates of Th^{3+} in the presence of carbon dioxide, methane, and oxygen are shown in Fig. 8. All of these gases react relatively quickly with Th^{3+} at rates comparable to the Langevin rate. Even at partial pressures below 10^{-8} torr, reactions occurring in the space between the ablation target and the trapping region significantly reduced the number of Th^{3+} ions loaded. To ensure sufficient loading and an adequate SNR for fluorescence measurement, 10^{-4} torr of helium was added to the system for each measurement. The loss rates measured here were in all cases significantly higher than the loss rate with only 10^{-4} torr of helium present.

The products of reaction between Th^{3+} and carbon dioxide, methane, and oxygen were identified using mass selective CEM detection. For these measurements, 2×10^{-8} torr of the test gas and 10^{-4} torr of helium buffer gas was introduced into the system. The ion trap was loaded a number of times. Each time the trap was loaded, we waited a short period ($\sim$1 s) for reactions to occur, performed a mass selection, and checked for the presence of ions. Since the rf power supply for our trap could not provide high-enough voltage to perform rigorous mass selection on singly ionized molecules, we were able to identify only doubly ionized molecules.

When either carbon dioxide or oxygen was present in the system, Th^{2+} and ThO^{2+} were found in the trap. Although thorium dioxide is chemically stable, no ThO_2^{2+} was detected with either gas. In a previous work with singly-ionized thorium, Johnsen *et al.* [22] found that oxidation occurs via the sequential reactions

$$Th^+ + O_2 \rightarrow ThO^+ + O \quad (5)$$

$$ThO^+ + O_2 \rightarrow ThO_2^+ + O. \quad (6)$$

They found that the first reaction proceeded quickly, with a rate coefficient of 6×10^{-10} cm^3 s^{-1}, whereas the rate of the second reaction was more than an order of magnitude lower, with a coefficient of 2×10^{-11} cm^3 s^{-1}.

Reactions between Th^{3+} and methane, CH_4, resulted in Th^{2+} and $ThCH_2^{2+}$. Special care was taken to properly identify $ThCH_2^{2+}$. Andrews and Cho [26] were able to create $ThCH_4$ by ablating thorium in a methane environment. However, Marçalo *et al.* [35] found that the only reaction channel between singly ionized thorium and methane is

$$Th^+ + CH_4 \rightarrow ThCH_2^+ + H_2. \quad (7)$$

Only 1 amu/e separates the mass-to-charge ratio of $ThCH_2^{2+}$ from $ThCH_4^{2+}$ and ThO^{2+}. By carefully mapping the voltage space in which ThO^{2+} and $ThCH_2^{2+}$ were stable, we were able to achieve the resolution necessary to correctly determine the product (see Fig. 9).

Once the reaction products were identified, we were able to measure how Th^{3+} evolved over time in the presence of each of these gases. The results are shown in Fig. 10 for

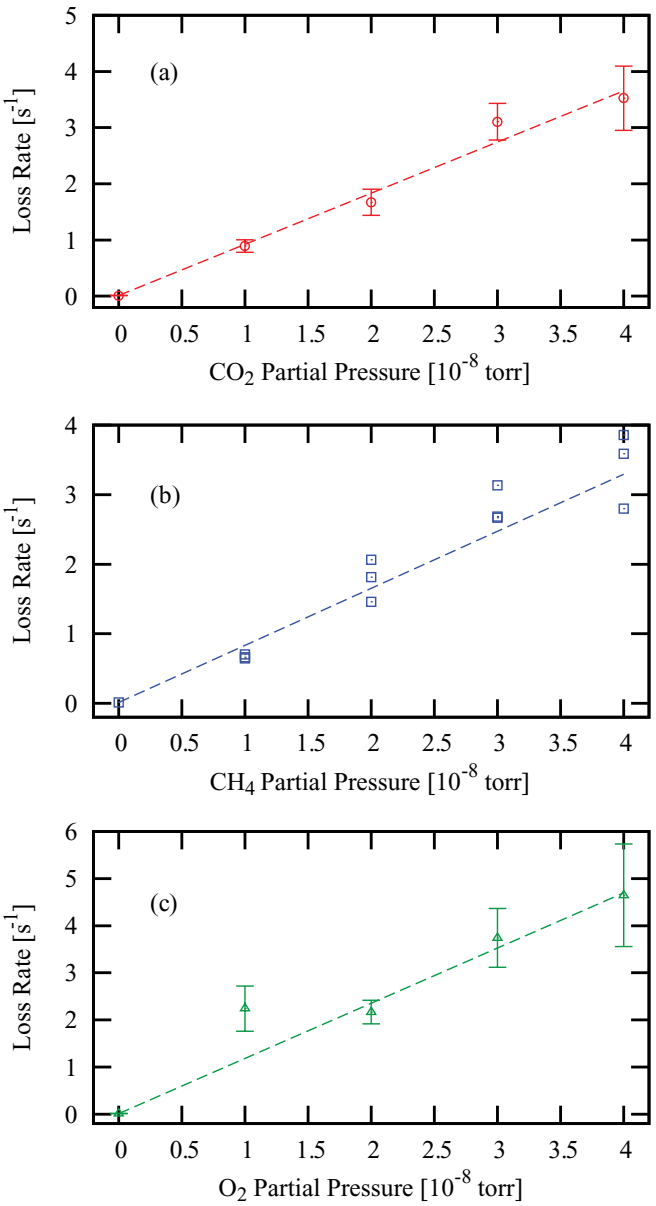

FIG. 8. (Color online) Th^{3+} loss rate in the presence of (a) carbon dioxide, (b) methane, and (c) oxygen. Measurements were made with 10^{-4} torr of helium buffer gas. The data point at zero pressure is the loss rate when only helium at 10^{-4} torr is present. Reaction rate coefficients for each case are listed in Table I.

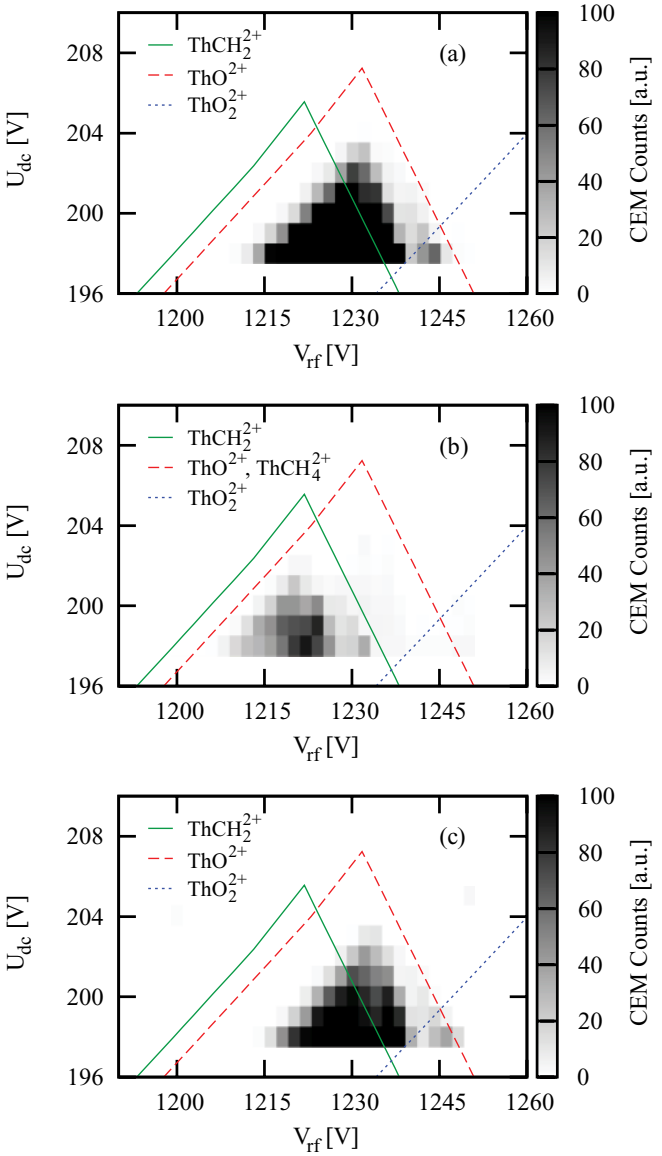

FIG. 9. (Color online) Doubly ionized thorium molecules. Ions are identified by comparing the voltage space in which they are stable to the theoretical stability region. (a) The reaction between Th^{3+} and carbon dioxide produces ThO^{2+}. (b) The reaction between Th^{3+} and methane produces Th^{2+}, which in turn reacts with methane to produce $ThCH_2^{2+}$. (c) The reaction between Th^{3+} and oxygen produces Th^{2+}, which in turn reacts with oxygen to produce ThO^{2+}.

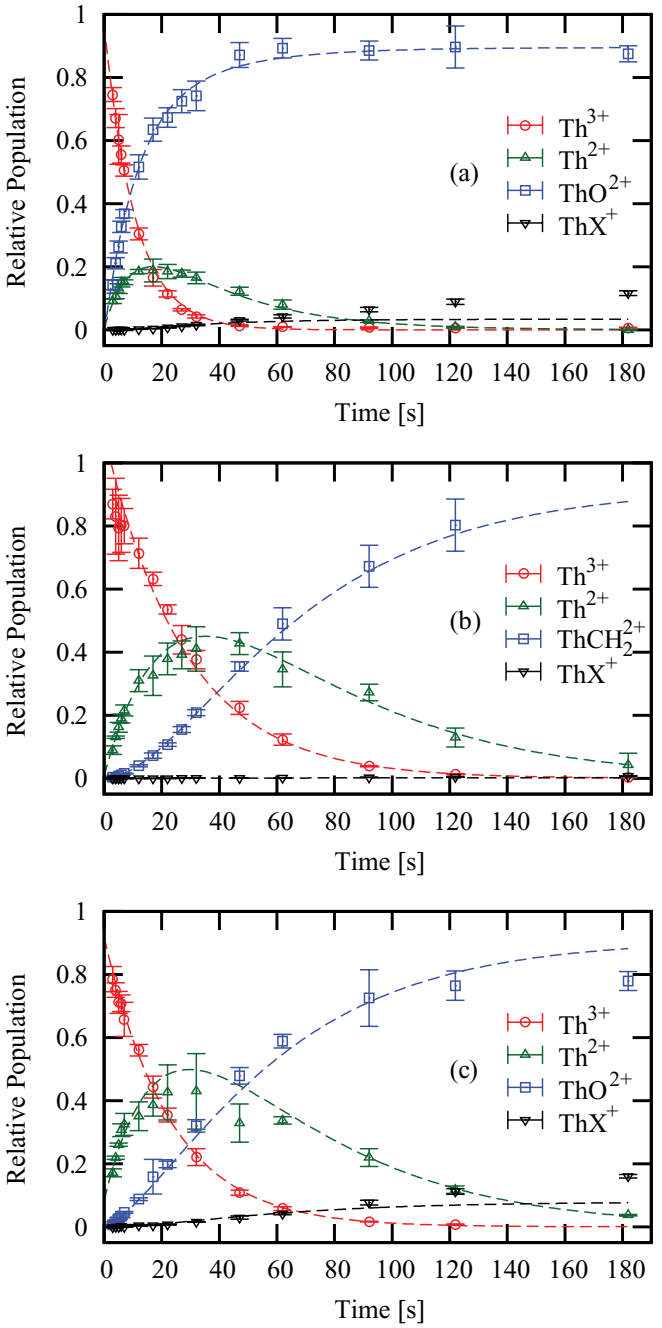

FIG. 10. (Color online) $^{232}Th^{3+}$ in the presence of (a) carbon dioxide, (b) methane, and (c) oxygen. The data are scaled according to the values given in Table II. The data sets are fit to the system of equations given in Eqs. (15)–(18).

carbon dioxide, methane, and oxygen. Each data point in these graphs represents the average and standard deviation of six measurements. For each measurement, the trap was loaded, and Th^{3+} was mass selected. A fluorescence measurement would be taken immediately after the mass selection. After the specified wait time, the ion of interest would be mass selected and the contents of the trap delivered to the CEM. The resulting CEM signal was normalized according to the initial fluorescence measurement. By normalizing the signal in this way, the impact of loading fluctuations on the data was minimized.

As was mentioned previously, the rf power supply for our trap could not provide high-enough voltage to perform rigorous mass selection on singly ionized molecules. However, by ramping the rf to its maximum voltage, we could isolate ions with mass-to-charge ratios greater than 156 amu/e. The only ions in the trap above that mass-to-charge ratio would be singly ionized thorium molecules. These are represented as ThX^+ in Fig. 10.

Direct comparison of the CEM signals of the various ions is of limited value since the gain of a CEM can vary from ion to ion. Ions with higher charge states experience a greater acceleration in the field created by the high negative bias at the

entrance of the dynode. These ions strike the dynode surface with greater energy, resulting in a higher initial emission of electrons. The CEM gain also depends on mass, as lighter ions tend to cause a larger response than more massive ones. The chemical nature of the ion can also play a role.

We verified several times that the Th^{3+} CEM signal was linear with measurements of total fluorescence over the dynamic range of both instruments. However, the specific slope of the relationship at any given time was highly sensitive to the background light level around the system. Curtains were employed to stabilize and minimize background light; however, small shifts in the curtains incurred while the system was prepared for data collection still had a noticeable effect.

In order to compare the relative populations of the various ions in the trap over time, we adopted a simple method for scaling the CEM data. The method is based on two assumptions. We assume first that ions are not lost from the trap over the period of investigation. This is reasonable given that the trap depth is on the order of 100 eV for the ions in question, while the exothermicity of the reactions is only on the order of a few eV. We further assume that the only ions present in the trap are those identified in our earlier search for the reaction products. Since our method of searching for reaction products focused only on products resulting from fast reactions, this assumption could lead to error when considering longer time scales. However, here we focus our attention on the rapid chemical kinetics that occur on short time scales.

To scale the data we consider the sum

$$N(t) = \sum_i \alpha_i n_i(t), \tag{8}$$

where N is the total trap population, and n_i and α_i are the fluorescence-normalized CEM signal and the CEM scaling factor for ion i, respectively. The sum is over all ion species present in the trap. The scaling factors are determined via a least-squares algorithm that attempts to make $N(t) = 1$ for all t. The data shown in Fig. 10 was scaled using this method. The scaling factors are given in Table II.

It is clear from Fig. 10 that the dynamics responsible for the appearance of ThO^{2+} in the presence of carbon dioxide differ from the dynamics that cause ThO^{2+} to arise in oxygen and that bring about $ThCH_2^{2+}$ in the presence of methane. Based on the identified products, the possible reactions between Th^{3+} and these gases can be written generally as

$$Th^{3+} + CO_2 \quad \begin{cases} \xrightarrow{\alpha_1} Th^{2+} + CO_2^+ \\ \xrightarrow{\alpha_2} ThO^{2+} + CO^+ \end{cases} \tag{9}$$

TABLE II. CEM scaling factors for Th^{3+} reaction data.

Species	Carbon dioxide	Methane	Oxygen
Th^{3+}	9.0	4.6	3.6
Th^{2+}	23.4	26.2	14.7
ThO^{2+}	36.8	—	12.7
$ThCH_2^{2+}$	—	53.9	—
ThX^+	20.5	30.0	39.3

$$Th^{3+} + CH_4 \quad \begin{cases} \xrightarrow{\beta_1} Th^{2+} + CH_4^+ \\ \xrightarrow{\beta_2} ThCH_2^{2+} + H_2^+ \end{cases} \tag{10}$$

$$Th^{3+} + O_2 \quad \begin{cases} \xrightarrow{\gamma_1} Th^{2+} + O_2^+ \\ \xrightarrow{\gamma_2} ThO^{2+} + O^+. \end{cases} \tag{11}$$

Here, α_i, β_i, and γ_i represent the relative probabilities of the reaction channels. The possible subsequent reactions with Th^{2+} can be summarized as

$$Th^{2+} + CO_2 \quad \begin{cases} \xrightarrow{\alpha_3} ThX^+ + \cdots \\ \xrightarrow{\alpha_4} ThO^{2+} + CO \end{cases} \tag{12}$$

$$Th^{2+} + CH_4 \quad \begin{cases} \xrightarrow{\beta_3} ThX^+ + \cdots \\ \xrightarrow{\beta_4} ThCH_2^{2+} + H_2 \end{cases} \tag{13}$$

$$Th^{2+} + O_2 \quad \begin{cases} \xrightarrow{\gamma_3} ThX^+ + \cdots \\ \xrightarrow{\gamma_4} ThO^{2+} + O. \end{cases} \tag{14}$$

No decay in the quantity of ThO^{2+} or $ThCH_2^{2+}$ is seen over the time scales investigated, so these can be treated as stable final products. Thus, from the above reaction equations, we can write a system of differential equations describing the chemical kinetics in each gas. For example, in carbon dioxide,

$$\frac{d}{dt}\,\mathrm{n}(Th^{3+}) = -k_1\,\mathrm{n}(Th^{3+}) \tag{15}$$

$$\frac{d}{dt}\,\mathrm{n}(Th^{2+}) = -k_2\,\mathrm{n}(Th^{2+}) + \alpha_1 k_1\,\mathrm{n}(Th^{3+}) \tag{16}$$

$$\frac{d}{dt}\,\mathrm{n}(ThO^{2+}) = \alpha_2 k_1\,\mathrm{n}(Th^{3+}) + \alpha_4 k_2\,\mathrm{n}(Th^{2+}) \tag{17}$$

$$\frac{d}{dt}\,\mathrm{n}(ThX^+) = \alpha_3 k_2\,\mathrm{n}(Th^{2+}). \tag{18}$$

Similar systems of equations can be written to describe the reaction dynamics in methane and oxygen.

To estimate the relative probabilities of the various reaction channels, the data of Fig. 10 was numerically fit to dynamic equations of the form shown above. Fits were performed in the order of the above equations. Once a value was obtained for a fitting parameter, that value was enforced on subsequent fits. The branching ratios that were determined in this fashion are given in Table III.

The values given in Table III can only be considered rough estimates of the actual branching ratios because of the uncertainties inherent in the CEM scaling procedure. They are given only to illustrate the general reaction dynamics. While reactions of Th^{3+} with methane and oxygen proceed predominantly via charge exchange, simultaneous charge exchange and chemical reaction is the dominant branch in reactions between Th^{3+} and carbon dioxide. Since methane

TABLE III. Branching ratios for thorium reactions.

Branching ratio	Carbon dioxide	Methane	Oxygen
$[\alpha,\beta,\gamma]_1$	0.36	0.89	1.0
$[\alpha,\beta,\gamma]_2$	0.78	0.0	0.09
$[\alpha,\beta,\gamma]_3$	0.10	0.0	0.08
$[\alpha,\beta,\gamma]_4$	0.44	0.94	0.83

TABLE IV. Purity specifications for research grade argon, ultrahigh purity hydrogen, and research grade neon used in reaction experiments. Values listed are in ppm. All gases were purchased from Airgas, Inc. and specifications are listed in the Airgas 2009 Product Catalog [30].

Gas	Minimum purity	CO_2	O_2	Hydrocarbons
Argon	99.9997%	<0.5	<0.2	<0.2
Hydrogen	99.999%	<0.5	<1	<0.5
Neon	99.999%	<0.5	<0.5	<0.5

has the highest ionization energy and lowest polarizability among hydrocarbons [36], the charge exchange reaction rates between other hydrocarbons and Th^{3+} are likely as high as those of methane.

It is worth considering whether impurities of these fast reacting gases could explain the Th^{3+} losses in the presence of argon, nitrogen, and hydrogen. CO_2, O_2, and CH_4 each react strongly with Th^{3+} at rates very close to the calculated Langevin rates. In order for these molecules to account for the observed loss rates in the other gases, they would have to be present as impurities at the 10^{-4} level reacting at the Langevin rate, considerably higher than the levels specified by the gas supplier (see Table IV). Furthermore, none of these molecules exhibited different reaction rates due to optical excitation of Th^{3+}, so their presence as impurities could not explain the reaction rates observed for argon and nitrogen. For these reasons, it is unlikely that impurities of the type measured to react at the Langevin rate are responsible for the losses observed for the slowly reacting gases.

VI. CONCLUSION

We have determined the effect of various gases on the trap lifetime of Th^{3+}. Reactions involving carbon dioxide, oxygen, and methane proceed at a rate near the classical Langevin limit. Although charge exchange reactions with them are exothermic, the reaction rate coefficients for nitrogen, hydrogen, and argon are orders of magnitude less than the Langevin rate. The reaction rate coefficient between Th^{3+} and helium provides a measure of the impurities in the buffer gas. The measurement of the coefficient here provides a standard against which the vacuum and buffer gas quality of future systems can be measured.

ACKNOWLEDGMENTS

We gratefully acknowledge Adam Steele, Corey Campbell, Alex Radnaev, and Alex Kuzmich for their assistance with this work, and we thank Ken Brown for valuable discussions. This work was supported by the Office of Naval Research (N000140911024) and the National Science Foundation (PHYS-1002550).

[1] B. R. Beck, J. A. Becker, P. Beiersdorfer, G. V. Brown, K. J. Moody, J. B. Wilhelmy, F. S. Porter, C. A. Kilbourne, and R. L. Kelley, Phys. Rev. Lett. **98**, 142501 (2007).
[2] E. Peik and C. Tamm, Europhys. Lett. **61**, 181 (2003).
[3] V. V. Flambaum, Phys. Rev. Lett. **97**, 092502 (2006).
[4] A. C. Hayes and J. L. Friar, Phys. Lett. B **650**, 229 (2007).
[5] X. T. He and Z. Z. Ren, J. Phys. G: Nucl. Part. Phys. **34**, 1611 (2007).
[6] X. T. He and Z. Z. Ren, Nucl. Phys. A **806**, 117 (2008).
[7] J. C. Berengut, V. A. Dzuba, V. V. Flambaum, and S. G. Porsev, Phys. Rev. Lett. **102**, 210801 (2009).
[8] C. J. Campbell, A. V. Steele, L. R. Churchill, M. V. DePalatis, D. E. Naylor, D. N. Matsukevich, A. Kuzmich, and M. S. Chapman, Phys. Rev. Lett. **102**, 233004 (2009).
[9] P. Langevin, Ann. Chim. Phys. **28**, 433 (1903).
[10] G. Gioumousis and D. P. Stevenson, J. Chem. Phys. **29**, 294 (1958).
[11] J. Troe, Chem. Phys. Lett. **122**, 425 (1985).
[12] D. O. Schissler and D. P. Stevenson, J. Chem. Phys. **24**, 926 (1956).
[13] F. H. Field, J. L. Franklin, and F. W. Lampe, J. Am. Chem. Soc. **79**, 2419 (1957).
[14] N. Boelrijk and W. H. Hamill, J. Am. Chem. Soc. **84**, 730 (1962).
[15] B. H. Mahan, J. Chem. Phys. **55**, 1436 (1971).
[16] R. Johnsen and M. A. Biondi, Phys. Rev. A **18**, 996 (1978).
[17] R. Johnsen and M. A. Biondi, Phys. Rev. A **20**, 87 (1979).
[18] R. Johnsen and M. A. Biondi, J. Chem. Phys. **73**, 190 (1980).
[19] H. M. Holzscheiter and D. A. Church, J. Chem. Phys. **74**, 2313 (1981).
[20] D. A. Church and H. M. Holzscheiter, Phys. Rev. A **40**, 54 (1989).
[21] E. W. McDaniel, *Ion-Molecule Reactions* (Wiley-Interscience, New York, 1970).
[22] R. Johnsen, F. R. Castell, and M. A. Biondi, J. Chem. Phys. **61**, 5404 (1974).
[23] H. M. Holzscheiter and D. A. Church, Phys. Lett. A **86**, 25 (1981).
[24] H. Chatham, D. Hils, R. Robertson, and A. C. Gallagher, J. Chem. Phys. **79**, 1301 (1983).
[25] D. A. Church, J. Mod. Opt. **39**, 423 (1992).
[26] L. Andrews and H. G. Cho, J. Phys. Chem. A **109**, 6796 (2005).
[27] F. G. Major and H. G. Dehmelt, Phys. Rev. **170**, 91 (1968).
[28] H. Wu and J. S. Brodbelt, Int. J. Mass Spectrom. Ion Processes **124**, 175 (1993).
[29] R. G. DeVoe, Phys. Rev. Lett. **102**, 063001 (2009).
[30] Airgas, Inc., *Airgas 2009 Product Catalog* (2009).
[31] R. K. Janev and H. Winter, Phys. Rep. **117**, 265 (1985).
[32] X. Fléchard, C. Harel, H. Jouin, B. Pons, L. Adoui, F. Frémont, A. Cassimi, and D. Hennecart, J. Phys. B: Adv. At. Mol. Opt. Phys. **34**, 2759 (2001).
[33] S. Knoop, M. Keim, H. J. Lüdde, T. Kirchner, R. Morgenstern, and R. Hoekstra, J. Phys. B: Adv. At. Mol. Opt. Phys. **38**, 3163 (2005).
[34] D. Bodewits and R. Hoekstra, Phys. Rev. A **76**, 032703 (2007).
[35] J. Marçalo, J. P. Leal, and A. P. de Matos, Int. J. Mass Spectrom. Ion Processes **157-158**, 265 (1996).
[36] D. R. Lide, *CRC Handbook of Chemistry and Physics*, 88th ed. (CRC Press, Boca Raton, FL, 2007).